nature physics

LETTERS

PUBLISHED ONLINE: 14 AUGUST 2017 | DOI: 10.1038/NPHYS4224

Current–phase relations of few-mode InAs nanowire Josephson junctions

Eric M. Spanton[1,2], Mingtang Deng[3,4], Saulius Vaitiekėnas[3,5], Peter Krogstrup[3], Jesper Nygård[3], Charles M. Marcus[3] and Kathryn A. Moler[1,2,6]*

Gate-tunable semiconductor nanowires with superconducting leads have great potential for quantum computation[1-3] and as model systems for mesoscopic Josephson junctions[4,5]. The supercurrent, *I*, versus the phase, ϕ, across the junction is called the current–phase relation (CPR). It can reveal not only the amplitude of the critical current, but also the number of modes and their transmission. We measured the CPR of many individual InAs nanowire Josephson junctions, one junction at a time. Both the amplitude and shape of the CPR varied between junctions, with small critical currents and skewed CPRs indicating few-mode junctions with high transmissions. In a gate-tunable junction, we found that the CPR varied with gate voltage: near the onset of supercurrent, we observed behaviour consistent with resonant tunnelling through a single, highly transmitting mode. The gate dependence is consistent with modelled subband structure that includes an effective tunnelling barrier due to an abrupt change in the Fermi level at the boundary of the gate-tuned region. These measurements of skewed, tunable, few-mode CPRs are promising both for applications that require anharmonic junctions[6,7] and for Majorana readout proposals[8].

In superconductor–normal–superconductor (SNS) Josephson junctions, the critical current is predicted to be quantized as $I_C = N\Delta_0/\hbar$ (refs 4,5), where N is the number of occupied subbands and Δ_0 is the superconducting gap, as long as N is sufficiently small and the junctions are short, ballistic and adiabatically smooth. This quantization shows the number of Andreev bound states or modes, each coming from a single occupied subband, that carry the supercurrent. Single-mode junctions are desirable for the observation of Majoranas. Quantized supercurrent has been difficult to realize experimentally, and it is difficult from transport measurements alone to determine which conditions for quantization are unmet. In transport measurements of proximitized InAs and InSb nanowires, critical currents are far below the expected quantized values for perfectly transmitting modes, and fluctuate with gate voltage[9–13]. Nanowire Josephson junction qubits also display similar fluctuations in the measured resonant frequency[6,7]. Here, we make direct, non-contact measurements (Fig. 1a) of Al/InAs nanowire/Al junctions (Fig. 1b,c) using an inductively coupled[14] scanning superconducting quantum interference device[15,16] (SQUID) to measure the CPR (Methods). The contact between Al and InAs nanowires is epitaxial[17], greatly reducing the presence of in-gap states[2]. In the low-temperature, few-mode limit, the shape of the CPR and its dependence on gate voltage, junction length and temperature yield unique insights into the number and transmission of Andreev bound states.

The vast majority of CPRs we measured were forward-skewed; their first maximum after zero was forward of a sine wave (Fig. 1d). Fourier transforms of the CPRs revealed that they were well described by a Fourier series with up to seven harmonics (for example, Fig. 1e). In the absence of time-reversal symmetry breaking, the theoretical CPR can be decomposed into a sine Fourier series[18]; fits to the experimental data include appropriate instrumental phase shifts (Methods, Supplementary Section 3).

The Fourier amplitudes (A_n) obtained by fitting the CPR characterize its shape. A_1 is the amplitude of the 2π-periodic component and is approximately I_C. The 'shape parameters' $a_n \equiv (-1)^{n+1}A_n/A_1$ characterize the shape of the CPR independent of its amplitude. Positive a_2 indicates a forward-skewed CPR; negative a_2 indicates a backward-skewed CPR. Higher-order terms yield more detailed information about the shape of the CPR and can be used to extract information about multiple modes, to compare with CPR theories, and to differentiate between the effects of elevated temperature and lowered transmission. Higher harmonics of the CPR can potentially reveal information about high-transmission modes even in junctions with many modes, similar to higher-order multiple Andreev reflections observed in superconducting point contacts[19,20] (Supplementary Section 7).

The amplitude and shape of the CPR of an $L = 150$ nm nanowire junction fluctuated as a function of applied bottom gate voltage, V_{BG}. The fluctuations were most dramatic close to depletion of the nanowire as seen in Fig. 2. The most forward-skewed CPR observed in this study and a backward-skewed CPR both occurred in the same gate-tuned junction (Fig. 2a). Fluctuations in A_1 remained similar in amplitude for all V_{BG} (Fig. 2b), while fluctuations in a_n decreased with increased V_{BG} (Fig. 2c) and with elevated temperature (Supplementary Section 1). The phase of the CPR remained constant for all gate voltages, indicating that the junction never underwent a 0 to π-junction transition (Fig. 2a).

A_n and a_n both displayed peaked behaviour near depletion, where we expect a single subband to be occupied (Fig. 3a,b). The peaks in both a_2 and A_n were asymmetric, with the side at more positive V_{BG} appearing more broad (Fig. 3a,b). The most forward-skewed CPR occurred in this peaked regime (Fig. 3c).

We observed a backward-skewed CPR only for a narrow gate voltage range in the gated junction, and never in ungated junctions (Fig. 4a). a_2 was negative in the backward-skewed region (Fig. 4c) and was nearly coincident with a minimum in A_1 (Fig. 4b).

[1]Stanford Institute for Materials and Energy Sciences, SLAC National Accelerator Laboratory, Menlo Park, California 94025, USA. [2]Department of Physics, Stanford University, Stanford, California 94305, USA. [3]Center for Quantum Devices and Station Q Copenhagen, Niels Bohr Institute, University of Copenhagen, Copenhagen DK-2100, Denmark. [4]State Key Laboratory of High Performance Computing, NUDT, Changsha 410073, China. [5]Department of Physics, Freie Universität Berlin, Arnimallee 14, 14195 Berlin, Germany. [6]Department of Applied Physics, Stanford University, Stanford, California 94305, USA. *e-mail: kmoler@stanford.edu

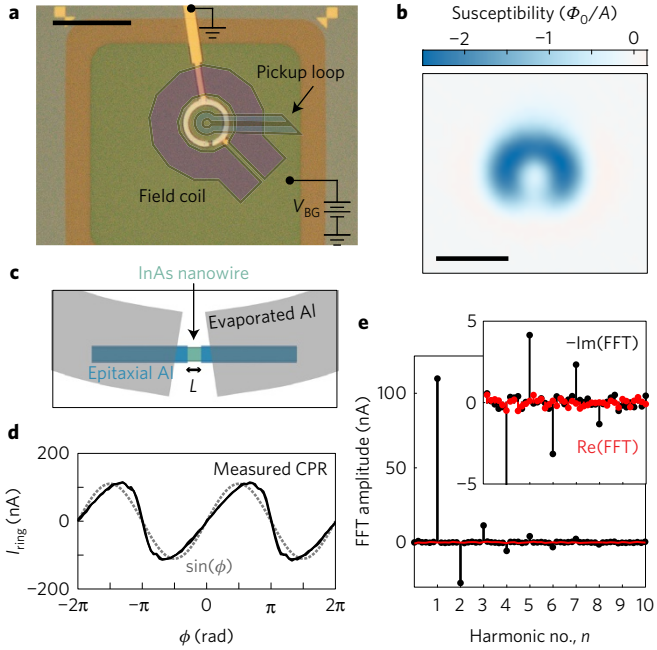

Figure 1 | Current–phase relation of a few-mode InAs nanowire junction as measured by scanning SQUID microscopy shows significant forward skew. a, Optical micrograph of an Al ring with a single epitaxial Al/InAs nanowire/Al junction and a sketch of the scanning SQUID geometry. The size of the ring was matched to couple inductively to the geometry of the SQUID's pickup loop (blue; used to measure the current flowing around the ring) and field coil (purple; used to apply a phase difference across the nanowire junction). We used an Au bottom gate to tune the density of one nanowire in some of the measurements. **b**, Local susceptibility image of a single-junction ring, showing the diamagnetic response of the evaporated Al ring. We used this signal to centre the SQUID's pickup loop over the centre of the ring. **c**, Schematic of the epitaxial Al/nanowire/Al junction. The InAs nanowire (green) was coated on all sides with epitaxial Al (blue). We etched the Al of a small length (L) of the nanowire to form the normal junction region. Evaporated Al (grey) forms the ring. **d**, An example of a measured CPR (black) of an $L = 150$ nm junction at $V_{BG} = 3.45$ V and $T = 30$ mK. The shape of the CPR is non-sinusoidal (a reference sine wave is presented in grey) and forward-skewed (the first maximum after $\phi = 0$ is forward of $\pi/2$). **e**, Real and imaginary fast Fourier transform (FFT) amplitudes (red and black, respectively) of the CPR taken from the interval $[-6\pi, 6\pi]$. The imaginary component (black) shows that the shape of this CPR is well described by a sine Fourier series with eight harmonics.

a_3 switched sign when a_2 was at its most negative. Our observation of a backward-skewed CPR cannot be explained by noise rounding, as in ref. 21, as the junction studied here was not near the hysteretic regime (Supplementary Section 4).

Junctions with different lengths (Fig. 5) exhibited a range of I_C and forward-skewness (Fig. 5a). A_1 did not depend strongly on the length of the junction (L) (Fig. 5b) and a_2 trended downward with increasing L, albeit with significant scatter (Fig. 5c). We detected no clear correlation between A_1 and a_2 (Supplementary Fig. 1), which suggests that variations in the Fermi level from junction to junction were responsible for fluctuations in the amplitude and shape of the CPR.

For SNS junctions in the short-junction limit (when L is much smaller than the superconductor's coherence length), each occupied subband (mode) leads to a single Andreev bound state whose properties depend only on its normal-state transmission (τ) (ref. 4). The short-junction limit holds for the junctions studied here except very close to the onset of a new subband, where a low Fermi velocity makes the junction in effect very long (Supplementary Section 6). The CPR is predicted to be sinusoidal when $T \sim T_C$ or when $\tau \ll 1$, but forward-skewed at low temperatures and high transmissions, as evident in the short-junction expression for the CPR:

$$I(\phi) = \frac{e\Delta_0(T)}{2\hbar} \sum_{p=1}^{N} \frac{\tau_p \sin(\phi)}{[1 - \tau_p \sin^2(\phi/2)]^{1/2}} \times \tanh\left(\frac{\Delta_0(T)}{2k_B T}[1 - \tau_p \sin^2(\phi/2)]^{1/2}\right) \quad (1)$$

where T is the temperature, k_B is the Boltzmann constant, $\hbar$ is the reduced Planck constant, $\Delta_0(T)$ is the superconducting gap, and e is the electron charge.

We can estimate the typical transmission (τ) from the skewness, a_2, and the number of modes (N) from the amplitude, A_1, assuming a value of T based on our mixing chamber temperature. For $V_{BG} > 4$ V in Fig. 2, $a_2 \approx 0.2$ and $A_1 \approx 100$ nA; we estimate that $\tau \approx 0.8$ and $N \approx 4$–5. For the CPRs measured on many junctions in Fig. 5, N varies from 0–10 and τ varies from 0.5–0.9 for CPRs with $A_1 > 10$ nA. Therefore, the junctions are in the few-mode regime and often have modes with very high transmission. Realistically, a junction would have an integer number of modes with different transmissions. Multi-mode fits to equation (1) could potentially resolve multiple values of τ_p and would be particularly sensitive to the presence of high-transmission modes (Supplementary Section 7).

Peaks in A_n versus gate voltage at low densities indicate resonant tunnelling behaviour (Figs 3 and 4). Equation (1) remains valid for a junction with tunnel barriers, with τ given by the Breit–Wigner transmission[4]:

$$\tau = \frac{\Gamma_L \Gamma_R}{(E_F - E_0)^2 + 1/4(\Gamma_L + \Gamma_R)^2} \quad (2)$$

where $\Gamma_{L,R}$ are tunnel rates into the left and right barriers, respectively, and E_0 is the energy of the resonance with respect to the Fermi energy, E_F. Equation (2) is valid for SINIS junctions only when $\Gamma_L + \Gamma_R \gg \Delta_0$ and shows that perfect transmission ($\tau = 1$) requires the left and right tunnel barriers to have identical tunnel rates. The most skewed CPR we observed, shown in Fig. 3c, fits well to equation (1) with four parameters: T, τ, a scaling parameter (ϵ), and a phase shift (ϕ_0). Fixing T to its measured value, 0.03 K, gives a good fit with ϵ and ϕ_0 consistent with our experiment, with a best-fit $\tau = 0.98$. Allowing T to vary gives a best-fit value of $T = 0.13$ K and $\tau = 1.00$ (Supplementary Section 2). A fit to equation (1) with two free τ gave best-fit values of $\tau_1 = 1.00$ and $\tau_2 = 0.0$ (Supplementary Section 2). These results indicate a single mode with perfect or nearly perfect transmission.

We attribute the high-transmission mode (Fig. 3c) to supercurrent through a resonant mode formed by symmetric, weak barriers. Perfectly symmetric tunnel barriers are unlikely to accidentally occur due to disorder-induced quantum dot behaviour, so their origin is more likely an intrinsic barrier. Symmetric barriers can exist at the epitaxial InAs/Al interface and at the border between etched and Al-coated regions of the nanowire (Fig. 1c). Different band bending at the etched and Al-coated surfaces can lead to different radial wavefunctions and subband occupation, resulting in an effective tunnel barrier (wavefunction mismatch).

Simulations that include wavefunction mismatch reproduce the essential features of Figs 2 and 3 (Supplementary Section 5). First, we simulated a two-dimensional InAs junction with delta-function barriers that depend on the difference in Fermi velocity between the superconductor and normal parts of the junction[5]. At low Fermi energy, the model shows peaked behaviour in A_n and a_n, indicating a single resonant mode with a highly forward-skewed CPR. When

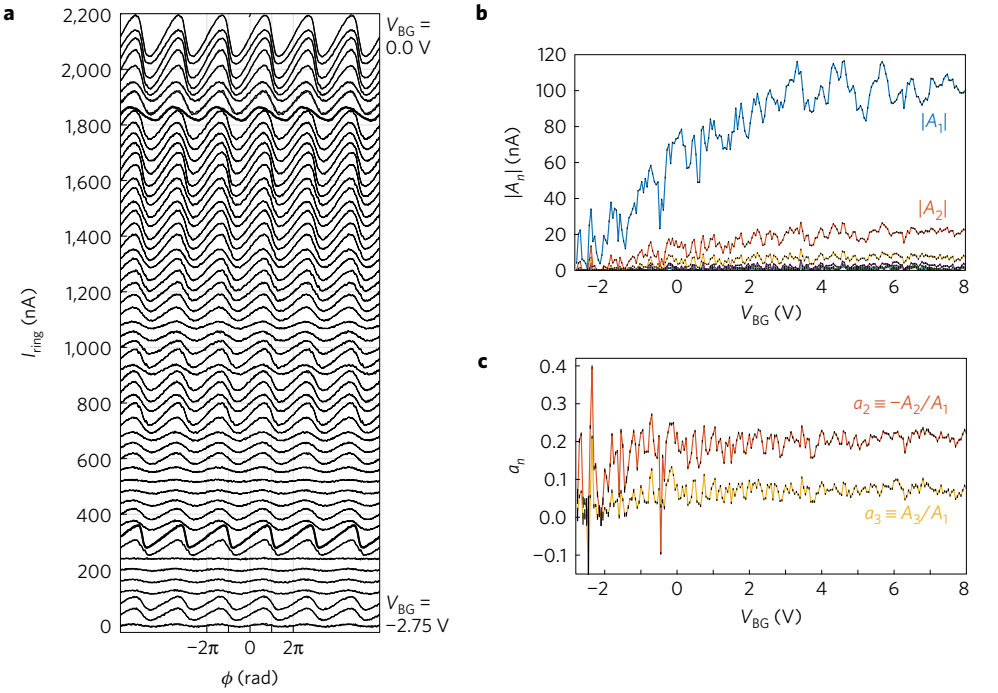

Figure 2 | Fluctuations in the forward skew and amplitude of the current–phase relation of a bottom-gated junction with gate voltage. a, CPRs (offset for clarity) versus bottom gate voltage (V_{BG}) for an $L = 150$ nm single-junction ring. $V_{BG} = -2.75$ V is close to depletion of the nanowire. The amplitude and shape of the CPR fluctuated strongly with gate voltage, particularly at the low gate voltages presented here. The most forward-skewed CPR and a backward-skewed CPR both occurred at low gate voltages (bold curves). **b**, Absolute value of the fitted harmonic amplitudes (A_n) versus V_{BG}. Non-zero harmonics for up to $n = 7$ were observed, and fluctuations were present for all of them. **c**, Fitted shape parameters ($a_n \equiv (-1)^{(n+1)} A_n/A_1$) versus V_{BG}. a_2 was positive except for a narrow range around $V_{BG} = -0.5$, indicating forward-skewed CPRs for most gate voltages.

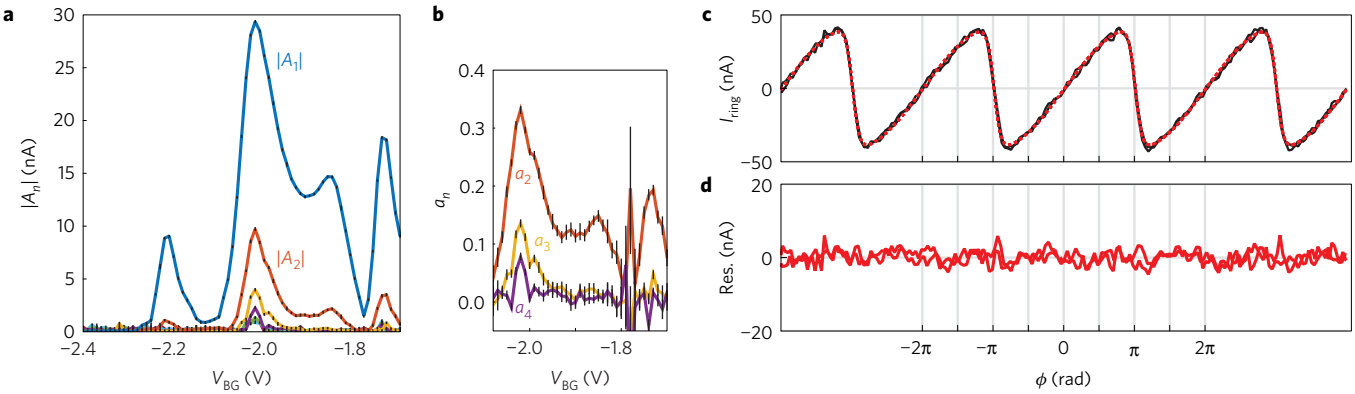

Figure 3 | Peak-like behaviour in the shape and skewness of the current–phase relation at low gate voltages. a,**b**, Harmonic amplitudes ($|A_n|$) (**a**) and shape parameters (a_n) (**b**) versus V_{BG} close to depletion with smaller gate voltage steps than Fig. 2. The shapes of the peaks in a_2 are cusp-like and asymmetric, consistent with simulations of a junction with wavefunction mismatch which leads to resonant tunnelling (Supplementary Section 5). The relative peak positions and heights in **a** and **b** are similar to those in Fig. 2 with an overall shift in V_{BG}, indicating that the features are robust to large sweeps in V_{BG}. **c**, Measured CPR (black) at $V_{BG} = -2.35$ V, from the gate sweep in Fig. 2. This CPR is the most forward-skewed CPR we observed and occurred in the low-density, peak-like regime. A free temperature fit, which allows for elevated electron temperature, yielded the following fitted parameters: $T = 0.13$ K, transmission $\tau = 1.00$, and a scaling factor (which scales I_C and A_n, but not a_n) that accounts for slight errors in the positioning of the SQUID $1 + \epsilon = 1.08$. A fit with fixed $T = 30$ mK and free ϵ gives $\tau = 1.00$. **d**, Residuals of the short-junction fit presented in **c**. The fit is of good quality with no obvious structure in the residuals.

many subbands are occupied at higher Fermi energies, the CPR's shape and amplitude fluctuate with Fermi energy. Second, we also performed tight-binding simulations, which use a more accurate cylindrical geometry, to capture the electron wavefunctions and the effects of wavefunction mismatch more directly. The tight-binding model also shows resonant single-mode CPRs at low Fermi energy and fluctuations when multiple subbands are occupied, showing that wavefunction mismatch is a likely candidate to describe the behaviour of forward-skewed CPRs in these nanowire junctions[22] (Supplementary Section 5). Our models do not include spin–orbit coupling, which is essential in describing the high-magnetic-field behaviour of InAs nanowire Josephson junctions. In the absence of a magnetic field, spin–orbit coupling can shift the energies of resonant Andreev levels and change the shapes of the resonant peaks, but each individual CPR is still described by equation (1) in the absence of interactions (ref. 23 and references therein, Supplementary Section 8).

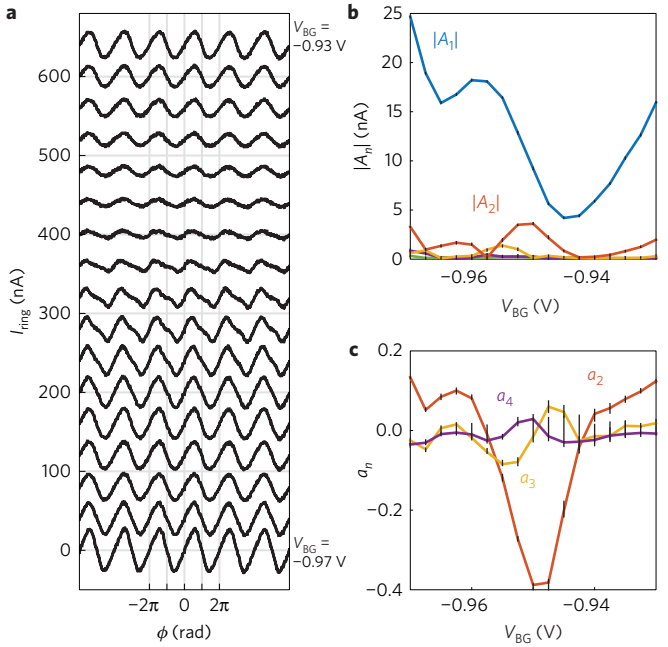

Figure 4 | Backward-skewed current–phase relations for a narrow range of gate voltages. a, CPRs versus V_{BG} with offsets for clarity, close to the region with backward-skewed CPRs (with a first maximum before $\phi = \pi/2$). **b**,**c**, Harmonic amplitudes ($|A_n|$) (**b**) and shape parameters (a_n) (**c**) versus V_{BG}. The first maximum of the shape precedes $\phi = \pi/2$ for a narrow range of gate voltages (**a**) and correspondingly a_2 becomes negative (**c**). The maximum backward-skewness is associated, but not completely coincident, with a local minimum in the amplitude, A_1 (**b**,**c**).

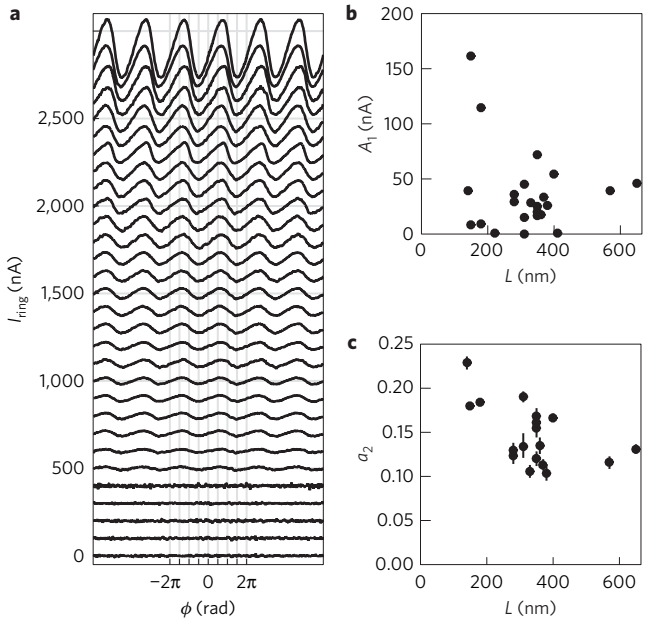

Figure 5 | The forward-skewness of the current–phase relation for many junctions with various lengths. a, CPRs of many InAs nanowire junctions with various lengths (dimensions listed in Supplementary Table 1), at low temperatures ($T \leq 50$ mK) and with no applied gate voltage. The CPRs are ordered by their overall amplitude. The shape and amplitude of the CPR varied substantially, and the degree of forward-skewness was not related to the amplitude. **b**, Fitted amplitude of the first harmonic (A_1) versus the nominal etched length of the junction (L). A_1 is approximately the critical current (I_C). A_1 does not show an obvious trend with length, therefore junction-to-junction variation (presumably of the chemical potential) is more important than L in determining A_1. **c**, Fitted shape parameter ($a_2 \equiv A_2/A_1$), which is directly proportional to the forward-skewness of the CPR, versus L. The forward-skewness weakly trended downward with longer junctions, indicating that the transmission of the junction was decreasing. We also detected large variations in forward-skewness for junctions of the same length. Error bars are 90% confidence intervals obtained from bootstrapping (see Methods).

The backward-skewed CPR (Fig. 4), however, does not arise in theories of short-junction SNS or resonant tunnelling behaviour (equations (1) and (2)). Interaction effects in the nanowire can lead to qualitatively similar backward-skewed CPRs and gate voltage dependence when the charging energy of the wire is finite, but not large enough to fully induce a 0–π junction transition[24,25] (Supplementary Section 8). The presence of both a fully transmitting single mode (which requires negligible charging energy) and a backward-skewed CPR implies that the charging energy of the junction is tuned by the gate voltage.

The shape of the CPR has important consequences for nanowire Josephson junction devices. Our observation of a single $\tau \sim 1$ mode that occurs at a peak in I_c, rather than a step, suggests that weak, symmetric tunnel barriers can form due to wavefunction mismatch in the nanowire. The resonance condition (equation (2)) leads to the maximum possible tunability of the skewness, and therefore the anharmonicity of the Josephson potential, with small gate voltages. Control of anharmonicity can tune nanowire-based qubits to a flux-qubit-like regime near $\phi = \pi/2$ (ref. 7). Our data also indicate that the likelihood of a non-sinusoidal CPR must be considered when attempting to extract the spatial distribution of current in Josephson junctions[26,27].

Inductive measurements of nanowire Josephson junctions with spin–orbit coupling[28], such as the Al/InAs nanowire/Al junctions studied here, or quantum spin Hall junctions[29] have been proposed as a readout mechanism for the parity of Majoranas. We have measured the CPR with the requisite sensitivity for non-contact readout of Majorana parity and observed the CPR of a single occupied subband that has close-to-perfect transmission. Challenges remain in realizing Majorana readout. First, the in-plane fields required to create Majoranas in InAs nanowires are a major technical challenge for scanning SQUID microscopy. Second, the timescale of the measurements presented here (up to tens of minutes) may not allow a measurement of a full CPR before environmental factors cause the parity to switch. Nevertheless, our sensitivity to such parity switching would allow us to use noise measurements to observe such environmental switching as long as the parity lifetime is longer than $\approx 10\,\mu s$.

Methods

Methods, including statements of data availability and any associated accession codes and references, are available in the online version of this paper.

Received 3 January 2017; accepted 3 July 2017; published online 14 August 2017

References

1. Mourik, V. *et al*. Signatures of Majorana fermions in hybrid superconductor-semiconductor nanowire devices. *Science* **336,** 1003–1007 (2012).
2. Chang, W. *et al*. Hard gap in epitaxial semiconductor–superconductor nanowires. *Nat. Nanotech.* **10,** 232–236 (2015).
3. Albrecht, S. M. *et al*. Exponential protection of zero modes in Majorana islands. *Nature* **531,** 206–209 (2016).
4. Beenakker, C. W. J. *Transport Phenomena in Mesoscopic Systems* 235–253 (Springer, 1992).
5. Furusaki, A., Takayanagi, H. & Tsukada, M. Josephson effect of the superconducting quantum point contact. *Phys. Rev. B* **45,** 10563–10575 (1992).

6. Larsen, T. W. *et al*. Semiconductor-nanowire-based superconducting qubit. *Phys. Rev. Lett.* **115,** 127001 (2015).
7. de Lange, G. *et al*. Realization of microwave quantum circuits using hybrid superconducting-semiconducting nanowire Josephson elements. *Phys. Rev. Lett.* **115,** 127002 (2015).
8. Hyart, T. *et al*. Flux-controlled quantum computation with Majorana fermions. *Phys. Rev. B* **88,** 035121 (2013).
9. Doh, Y.-J. *et al*. Tunable supercurrent through semiconductor nanowires. *Science* **309,** 272–275 (2005).
10. Günel, H. Y. *et al*. Supercurrent in Nb/InAs-nanowire/Nb Josephson junctions. *J. Appl. Phys.* **112,** 034316 (2012).
11. Abay, S. *et al*. Quantized conductance and its correlation to the supercurrent in a nanowire connected to superconductors. *Nano Lett.* **13,** 3614–3617 (2013).
12. Nilsson, H. A., Samuelsson, P., Caroff, P. & Xu, H. Q. Supercurrent and multiple Andreev reflections in an InSb nanowire Josephson junction. *Nano Lett.* **12,** 228–233 (2011).
13. Li, S. *et al*. Coherent charge transport in ballistic InSb nanowire Josephson junctions. *Sci. Rep.* **6,** 24822 (2016).
14. Jackel, L. D., Webb, W. W., Lukens, J. E. & Pei, S. S. Measurement of the probability distribution of thermally excited fluxoid quantum transitions in a superconducting ring closed by a Josephson junction. *Phys. Rev. B* **9,** 115–118 (1974).
15. Sochnikov, I. *et al*. Direct measurement of current-phase relations in superconductor/topological insulator/superconductor junctions. *Nano Lett.* **13,** 3086–3092 (2013).
16. Sochnikov, I. *et al*. Nonsinusoidal current-phase relationship in Josephson junctions from the 3d topological insulator HgTe. *Phys. Rev. Lett.* **114,** 066801 (2015).
17. Krogstrup, P. *et al*. Epitaxy of semiconductor–superconductor nanowires. *Nat. Mater.* **14,** 400–406 (2015).
18. Golubov, A. A., Kupriyanov, M. Yu. & Il'Ichev, E. The current-phase relation in Josephson junctions. *Rev. Mod. Phys.* **76,** 411–469 (2004).
19. Scheer, E., Joyez, P., Esteve, D., Urbina, C. & Devoret, M. H. Conduction channel transmissions of atomic-size aluminum contacts. *Phys. Rev. Lett.* **78,** 3535–3538 (1997).
20. Della Rocca, M. L. *et al*. Measurement of the current-phase relation of superconducting atomic contacts. *Phys. Rev. Lett.* **99,** 127005 (2007).
21. English, C. D. *et al*. Observation of nonsinusoidal current-phase relation in graphene Josephson junctions. *Phys. Rev. B* **94,** 115435 (2016).
22. Groth, C. W., Wimmer, M., Akhmerov, A. R. & Waintal, X. Kwant: a software package for quantum transport. *New J. Phys.* **16,** 063065 (2014).
23. Dell'Anna, L., Zazunov, A., Egger, R. & Martin, T. Josephson current through a quantum dot with spin-orbit coupling. *Phys. Rev. B* **75,** 085305 (2007).
24. Vecino, E., Martín-Rodero, A. & Levy Yeyati, A. Josephson current through a correlated quantum level: Andreev states and π junction behavior. *Phys. Rev. B* **68,** 035105 (2003).
25. Lee, E. J. H. *et al*. Spin-resolved Andreev levels and parity crossings in hybrid superconductor-semiconductor nanostructures. *Nat. Nanotech.* **9,** 79–84 (2014).
26. Hart, S. *et al*. Induced superconductivity in the quantum spin Hall edge. *Nat. Phys.* **10,** 638–643 (2014).
27. Allen, M. T. *et al*. Spatially resolved edge currents and guided-wave electronic states in graphene. *Nat. Phys.* **12,** 128–133 (2016).
28. Alicea, J., Oreg, Y., Refael, G., von Oppen, F. & Fisher, M. P. A. Non-Abelian statistics and topological quantum information processing in 1D wire networks. *Nat. Phys.* **7,** 412–417 (2011).
29. Fu, L. & Kane, C. L. Josephson current and noise at a superconductor/quantum-spin-Hall-insulator/superconductor junction. *Phys. Rev. B* **79,** 161408 (2009).

Acknowledgements

We thank S. Hart, J. Kirtley and C. Beenakker for useful discussions and C. Watson, Z. Cui and I. Sochnikov for useful discussions and experimental assistance. The scanning SQUID measurements were supported by the Department of Energy, Office of Basic Energy Sciences, Division of Materials Sciences and Engineering, under Contract No. DE-AC02-76SF00515. Nanowire growth and device fabrication was supported by Microsoft Project Q, the Danish National Research Foundation, the Lundbeck Foundation, the Carlsberg Foundation, and the European Commission. C.M.M. acknowledges support from the Villum Foundation.

Author contributions

P.K. and J.N. developed the nanowire materials, M.D. and S.V. fabricated the devices and E.M.S. performed the scanning SQUID measurements, analysed the data, and performed simulations. E.M.S. and K.A.M. wrote the manuscript with input from all coauthors.

Additional information

Supplementary information is available in the online version of the paper. Reprints and permissions information is available online at www.nature.com/reprints. Publisher's note: Springer Nature remains neutral with regard to jurisdictional claims in published maps and institutional affiliations. Correspondence and requests for materials should be addressed to K.A.M.

Competing financial interests

The authors declare no competing financial interests.

Methods

InAs nanowires were grown along the $[0001]_B$ direction and Al was deposited epitaxially to fully coat the nanowires[17]. A length, L, of the coated nanowire was etched to form a Josephson junction. We evaporated Ti/Al (5 nm/120 nm) *ex situ* to form the ring geometry required for CPR measurements. We measured the dimensions of the nanowires using scanning electron microscopy after the scanning SQUID measurements (Supplementary Fig. 2 and Supplementary Table 1).

We measured three samples, each with many single-junction rings, in a dilution refrigerator. In the gated junction, a gold bottom gate made of Ti/Au (5 nm/20 nm) with a AlO_x dielectric (40 nm) was used to tune the density of the nanowire. A number of devices were hysteretic; scanning electron microscopy revealed that they were under-etched (inset of Supplementary Section 4). We used a SQUID microscope in a dilution refrigerator with a nominal base temperature of ∼30 mK (refs 30,31). Temperatures were measured at the mixing chamber plate using a Rox thermometer. Data in the main text were all taken at $T < 50$ mK. We centred the scanning SQUID's pickup loop and field coil over the ring using the diamagnetic response of the evaporated Al to navigate, measured by applying an a.c. current through the field coil and standard lockin techniques (Fig. 1b). With the SQUID centred over the ring, we swept the current through our local field coil (I_{FC}) sinusoidally at ≈200 Hz and recorded the flux through the SQUID's pickup loop (Φ_{PU}) (Fig. 1a). We set the amplitude of I_{FC} to thread multiple flux quanta through the ring. We subtracted linear and experimental background from the measured Φ_{PU} versus I_{FC} to account for the diamagnetic response of the ring and imperfect geometric cancellation of the applied local field.

In single-junction rings (Fig. 1a), the CPR can be directly measured inductively as long as the self-inductance of the ring is small, $L_{self} < \Phi_0/2\pi I_c$, where Φ_0 is the superconducting flux quantum[14]. We converted measured Φ_{PU} versus I_{FC} to I versus ϕ (the CPR) using the periodicity of the signal and calculations of the mutual and self-inductances[32]. Although we included corrections for self-inductance effects in the conversion, they were not important in determining the shape of the CPR because the (non-shorted) junctions were always in the limit of $\beta = 2\pi L_s I_C/\Phi_0 \ll 1$. We confirmed our calculation of the self-inductance by measuring the height of steps in the response of hysteretic rings (Supplementary Section 4). Errors in centring the SQUID's pickup loop over the ring of a few micrometres would result in a systematic error of ≈10% in the extracted current and Fourier components A_n. The shape parameters a_n, however, are insensitive to this form of systematic error. We fitted both forward and backward sweeps of the CPR to extract their Fourier components. We fit the CPRs presented in Figs 2–4 using:

$$I(\phi) = \begin{cases} \sum_{n=1}^{N} A_n \sin(n(\phi + \phi_{FW})) & \text{if } d\phi/dt > 0 \\ \sum_{n=1}^{N} A_n \sin(n(\phi + \phi_{BW})) & \text{if } d\phi/dt < 0 \end{cases} \quad (3)$$

which fully accounted for the shape of the CPR. The phase shifts between forward and backward sweeps ($\phi_{bw,fw}$) were subtracted from ϕ in the figures presented in the main text. In Fig. 5, some CPRs exhibited phase shifts between harmonics. The harmonics were shifted in opposite directions for forward and backward sweeps, indicating that they were instrumental rather than intrinsic to the junction (see Supplementary Methods). Phase shifts between harmonics were not present in the CPRs in Figs 2–4, as is evident in the lack of an out-of-phase component in the fast Fourier transform (Fig. 1e). The errors bars in Figs 2–5 are 90% confidence intervals obtained from bootstrapping.

Data availability. The data that support the findings of this study are available from the corresponding author on reasonable request.

References

30. Gardner, B. W. *et al*. Scanning superconducting quantum interference device susceptometry. *Rev. Sci. Instrum.* **72,** 2361–2364 (2001).
31. Huber, M. E. *et al*. Gradiometric micro-SQUID susceptometer for scanning measurements of mesoscopic samples. *Rev. Sci. Instrum.* **79,** 053704 (2008).
32. Brandt, E. H. Thin superconductors and SQUIDs in perpendicular magnetic field. *Phys. Rev. B* **72,** 024529 (2005).